Journal of Microscopy, Vol. 207, Pt 3 September 2002, pp. 180–190
Received 20 February 2002; accepted 8 July 2002

Analytical electron microscopy as a tool for accessing colloid formation process in natural waters

C. MONDI*, K. LEIFER†, D. MAVROCORDATOS*[1] &
D. PERRET*[2]

*Institut de Chimie Minérale et Analytique, Université de Lausanne, CH-1015 Lausanne, Switzerland
†Institut de Micro-Optoélectronique, Ecole Polytechnique Fédérale, CH-1015 Lausanne, Switzerland

Key words. Analytical electron microscopy, colloid, iron, line scan, natural aquatic system, organic matter, quantification, TEM-EDS, TEM-EELS, TEM-ESI.

Summary

Analytical electron microscopy was used to characterize aquatic iron-rich colloids. We focused our attention on a redox transition medium in the drainage water of a peat soil. In the anoxic peat water, observations by transmission electron microscopy and associated energy dispersive analyses (TEM-EDS) highlight the presence of spherical entities (~100–600 nm), containing only traces of iron. The increase of dissolved oxygen concentration favours the formation of iron oxy(hydr)oxides. In the oxygenated drain, particles with the same morphology and size range are present. Statistical TEM-EDS analyses show that they represent the only colloidal form of iron in the drain samples. Nevertheless, although Fe–K peaks appear clearly on EDS spectra, the proportion of iron in these colloids reaches at most 4% at. (whereas C + O > 90% at.). Structural information completes this study. Both electron spectroscopic imaging (ESI) and electron energy-loss spectroscopy (EELS) reveal the disparity between element distributions within the drain entities. Iron and calcium are preferably distributed on the outer sphere of the particle, whereas carbon and oxygen follow the theoretical variation of the signal intensity within a plain sphere. The implication of organic matter as nucleation site for iron precipitation is spectacularly demonstrated by the presence of nanometre-sized iron-rich phases highlighted by EELS line scans.

Introduction

The degradation of the quality of water resources represents a great threat to the environment and human health. Numerous studies on pollutant transport highlight the role of colloids, naturally occurring entities in the nanometre to micrometre size range (Tessier, 1992; McCarthy & Degueldre, 1993; Stumm, 1993). Hydrous iron oxides, which are ubiquitous in natural waters, are particularly efficient heavy metal scavengers. Depending on the physico-chemical conditions of the milieu, they may trap pollutants, aggregate and sediment, or dissolve, and then release pollutants. On the other hand, karstic aquifers are particularly sensitive to pollution because of rapid water flow circulation limiting natural remediation. Their predominance as water resources in many calcareous geological areas still forces their use. The study of the colloidal forms of iron in such water systems is therefore compulsory when investigating contaminant dispersion. However, such studies are scarce in the literature, above all at the scale of the individual particle.

In a previous study (Mavrocordatos *et al.*, 2000), we addressed this lack of information by assessing the particular transport behaviour of iron colloids in a karst aquifer. We showed that the circulation of iron colloids does not coincide with the water flow and that they may be caught within the complex channel network of the aquifer. To refine our understanding of the behaviour of iron colloids in the karst, the origin of these colloids was investigated. We related it to peat soils, which cover the karst network. As revealed by electron microscopy, no colloidal iron was detected in the peat pore water. However, modification of the physico-chemical conditions in the oxygenated drainage water of these soils lead to iron oxidation and precipitation. Fe-containing colloids are then transported in the river that collects drained water, down to a sinkhole to the karst. To understand their evolution in the karst, we asked the following questions. What is the intimate nature of these Fe-rich particles? How do they form under the contrasting conditions that prevail between the peat and the river?

Our present work, based on analytical electron microscopy (AES), attempts to answer these questions. Energy dispersive spectrometry (EDS) and electron energy-loss spectrometry

Correspondence: Dr C. Mondi, Laboratoire de Minéralogie – Cristallographie (LMCP), UMR 7590 CNRS, Universités Paris VI et VII, IPGP, 4, place Jussieu, case 115, F-75252 Paris Cedex 05, France. Tel.: +33/(0)1 44 27 50 59; fax: + 33/(0)1 44 27 37 85; e-mail: christine.mondi@lmcp.jussieu.fr
Present addresses: [1]EAWAG, CH-8600 Dübendorf, Switzerland and [2]IATE, Ecole Polytechnique Fédérale, CH-1015 Lausanne, Switzerland.

(EELS) were used in combination to extract information on these colloids at the micrometre and nanometre-scales. In a first step, a general survey on the morphology, size range and composition of Fe-rich globules was performed by means of TEM-EDS. Easy to use and rapid, this technique was perfectly adapted to our heterogeneous samples and allowed us to highlight the colloids of interest. In addition, EELS line scans and electron spectroscopic imaging (ESI) were used to detail element distributions within these colloids. This approach allowed us to ascertain direct association between organic matter and iron precipitates.

Experimental

Studied area and sampling

The studied area is located in the Swiss Jura mountains, in the Vallée-des-Ponts (20 km North of Neuchâtel, Switzerland), a flat valley covered by peat bogs at an altitude of around 1100 m. Artificial drains remaining from previous peat exploitation collect peat pore waters and transport them to a river, the Bied Brook. The river flows into a main sinkhole entering the karstic aquifer. After travelling nearly 4 km through the karst, the water rises as a unique spring, the Noiraigue (altitude: 740 m). One piezometer was installed to collect peat pore waters in the vicinity of the drainage system. Drain and river waters were sampled, respectively, in the drain (collecting chamber), at the outlet of the drain and a few metres away from the outlet. TEM specimens were prepared within 4–8 h after sampling. Details on the site can also be found in previous studies (Atteia & Kozel, 1997; Mavrocordatos *et al.*, 2000).

TEM specimen preparation

Specimens for electron microscopy were prepared on TEM grids (Cu 200 mesh; collodion covered, carbon coated) by a non-disturbing ultracentrifugation procedure described elsewhere (Lienemann *et al.*, 1998). TEM grids (Cu 400 mesh) covered by a SiO film (SPI® supply) were also used to avoid background carbon signal in the electron energy loss spectra. Schematically, raw samples are ultracentrifuged in tubes containing TEM grids, in a swing-out rotor (135 000 g, 1 h). According to Stokes' law, these conditions allow for the quantitative recovery of spherical particles with a size larger than 30 nm and a density above 1.1 g cm^{-3}. For peat samples, another specimen preparation method was also used. Directly on the field, after sample collection in a glove bag under nitrogen atmosphere, the solution is mixed with a fresh mixture of Nanoplast® (Nanoplast: sample = 1 : 10 (V:V)), a water-soluble embedding resin (Bachhuber & Frösch, 1983), and centrifuged above TEM grids placed on an horizontal disc (Perret *et al.*, 1991). This method guarantees that morphological artefacts or oxygenation during specimen preparation are avoided (Lienemann *et al.*, 1998).

Analytical electron microscopy

TEM-EDS A transmission electron microscope (Philips CM12, source W) coupled to an energy dispersive spectrometer (EDAX; DX-4 analyser) was used to determine the element composition of particles present in the peat pore waters, in the drain and in the river. EDS spectra were collected between 0 and 10 keV with a Si(Li) X-ray detector equipped with a super ultra-thin window (SUTW 0.3 μm thick). This window allows the detection of low energy X-rays including boron (Z = 5). An acceleration voltage of 80 keV and a condenser aperture of 100 μm were used to generate a typical spot size of 400 nm (about the size of the colloids of interest). Microscope-induced hydrocarbon contamination was reduced by using an ion-getter pump and liquid-nitrogen trap, ensuring a low partial pressure of hydrocarbons in the vicinity of the specimen. Organic specimens are known to easily introduce hydrocarbon contaminants, as they outgas in the vacuum. An offset of carbon concentration due to specimen-borne contamination may thus exist. Nevertheless, as the different particles are on the same grid and analysis conditions are similar, changes of carbon concentration from one particle class to the next should be systematic. Spectra were acquired with a live time of 100 s. The specimen was tilted at 20°. The atomic percentage of each element was calculated using the Cliff–Lorimer Eq. (1), extended to the number of analysed elements (C, O, Al, Si, K, S, P, Ca, Fe):

$$\frac{C_A}{C_B} = k_{AB}\frac{I_A}{I_B} \quad (1)$$

where $C_{A,B}$ = atomic proportions of elements A and B, $I_{A,B}$ = above-background K_α line intensities of elements A and B, and k_{AB} = Cliff–Lorimer factor.

k_{AB} factors were approximated using a theoretical cross-section (Mott–Massey). This method yields less precise atomic proportions than for measured k_{AB} factors. Nevertheless, the theoretical k_{AB} factors yield a rapid estimate of the composition of the analysed entities and results accurate within ± 10–20% (Williams & Carter, 1996). Furthermore, the Cliff–Lorimer equation neglects absorption effects. Especially when comparing the concentrations of transition with light elements, the influence of X-ray absorption on the computed concentrations has to be verified. In the OM-FeCa entities, the transition light element concentration (C + O) of 93% changes by ±1.5% at. when specimen thickness is varied by 200 ± 200 nm due to absorption correction, assuming a density of the entities of 2 g cm^{-3} (the density may range between 1 and 3.8 g cm^{-3} for organic matter and iron hydroxide, respectively). This value is within the range of concentration fluctuation that was observed from one particle to another (of the same class) and therefore does not influence the particle classification that is carried out in Table 2. We performed EDS analyses to classify our pool of colloidal matter into distinct classes of colloid types. After a first selection on the basis of their element

fingerprint and morphology, intensities of EDS peaks were used to estimate the relative concentration of elements in each type of particle. The carbon and oxygen signals originating from the collodion/carbon supporting film were subtracted by acquiring the signal of carbon and oxygen around the colloidal entities under identical conditions of analysis. We supposed that electron absorption in the particle is negligible, so that $I_{colloid} = I_{colloid+film} - I_{film}$. The precision of these results was sufficient for our study.

To obtain the unbiased distribution of the colloid types in water samples we used a statistical approach. Lienemann *et al.* (1998) showed that the distribution of colloids on TEM grids prepared by ultracentrifugation is directly correlated to the mass concentration of colloids in the suspension. On this basis, we selected evenly distributed areas of 64 μm^2 on TEM grids. The element composition of individual colloids and aggregates in each area was then analysed by EDS. Entities were discriminated into classes according to their composition and size. The aggregates were recorded as single particles, i.e. the composition of each particle in the aggregate contributes to the overall composition of the assemblage. The spot size was fixed at 400 nm for entities smaller than 500 nm and was adapted to the size of larger entities.

TEM-ESI Iron, calcium and oxygen element maps were obtained with an energy-filtered transmission electron microscope (EF-TEM Zeiss CEM902, source W, 80 keV) equipped with a Castaing–Henry filter in electron spectroscopic imaging (ESI) mode. River specimens were prepared by ultracentrifugation and deposited on collodion/carbon-coated TEM grids as described above. The three-window method was applied (with an energy window $\Delta = 13$ eV) in order to extrapolate and subtract the background ($A \times E^{-r}$). A relatively short acquisition time (24 s for each image) allowed the element information to be recorded without inducing beam damage to the microparticles or specimen drift. The deconvolution methods used for EELS to take into account multiscattering effects could not be applied. Reimer (1995) indicated that specimen thickness must be smaller or of the order of the mean free path of plasmon losses, which is about 80 nm in biological sections (rich in light elements) for 80 keV electrons.

TEM-EELS To follow chemical changes at the nanometre scale, profile analyses were performed on a high resolution TEM (Hitachi HF-2000, source field emission gun, 200 keV) equipped with a parallel electron energy loss spectrometer (PEELS – Gatan 666). In order to quantify precisely the carbon element content of the colloids, special attention was paid to hydrocarbon contamination. High vacuum in the column of the microscope and liquid-nitrogen trap reduce to a large extent microscope-induced hydrocarbon contamination of the specimen. These precautions, however, are not sufficient to avoid specimen-borne hydrocarbon contamination. This has to be taken into account when analysing organic specimens. We minimized this contamination by liquid-nitrogen cooling of the specimen during microscopy, which reduces the migration of hydrocarbons on the surface of the specimen. Cooling the specimen helped also to stabilize it under the electron beam and avoid specimen degradation. The spectral series were recorded with an acquisition time of 1 s spectrum^{-1}. This dwell time was optimized to acquire a sufficient signal intensity and to limit beam damage. Resolution in the line-scans was limited by the electron probe diameter of 1.5 nm (FWHM), as the spatial distance between neighboured spectra is 1 nm. The spatial resolution is further reduced by scattering of electrons in the specimen. Nevertheless, for a light matrix with a density of 2 g cm^{-3}, the electron probe diameter averaged between entrance and exit surface is smaller than 3 nm for the specimen thicknesses studied here (close to 120 nm). Therefore, the measured entity size of 7–23 nm on Fig. 5 is real and not due to electron beam broadening. Furthermore, we have measured the specimen drift of 2 nm mn^{-1} at the acquisition conditions. The total acquisition time of one line scan is about 2.5 min. This means that the specimen drift during a scan on a typical entity, with a size of about 120 nm, is smaller than 1 Å between neighboured spectra and therefore is negligible for the interpretation of our results. Moreover, during our EELS line scans experiment, we also collected spectra on the SiO supporting film around the colloidal entity, so that we were sure to have analysed both sides of the colloid. The convergence angle was $\alpha = 2$ mrad. The collection angle was $\beta = 50$ mrad. Two programs were developed for signal processing, the first for recording the spectra during line-scan acquisition, the second for the evaluation of the large spectrum series and the extraction of edge intensities (Leifer *et al.*, 2000).

Spectra were recorded from 200 to 1000 eV to determine the C-K edge (284 eV), the O-K edge (532 eV), the Fe-$L_{2,3}$ edge (708 eV) and the Ca-$L_{2,3}$ edge (346 eV) intensity. The zero loss peak (elastic electrons) and the plasmon region ($\approx 10^4\times$ more intense than the ionization edges of the elements) were acquired separately at each analysis point to estimate the specimen thickness (spectra recorded from 0 to 200 eV). Atomic percentages C_i were obtained using Eq. (2) stored in the Gatan EL/P 3.0 software:

$$C_i = \frac{I_i/\sigma_i}{\sum_j I_j/\sigma_j} \times 100 = \frac{A_i}{\sum_j A_j} \times 100 \qquad (2)$$

where C_i = atomic percentage of element i, I_i = ionization edge intensity of element i, after background subtraction, σ_i = partial cross-section of element i and A_i = number of atoms of element i.

Background subtraction was performed using a power-law model ($I = A \times E^{-r}$). A relatively large window ($\delta = 25$ eV) was used to model the background and extrapolate it under each edge. Ionization edges were integrated over an energy window $\Delta = 35$ eV to calculate their intensity I_i. Because the Ca-$L_{2,3}$ edge raises just after the C-K edge, we do not apply the same background and quantification intervals for the extraction

of the Ca edge intensity. We found the optimum background and quantification intervals (respectively $\delta = 10$ eV and $\Delta = 17$ eV) by comparing the results obtained by this method to the edge intensities obtained using Fourier-ratio deconvolution methods (program stored in the Gatan proprietary software). The partial cross-sections σ_i were calculated according to the algorithms SigmaL for Fe-$L_{2,3}$ and Ca-$L_{2,3}$ edges, and SigmaK for C-K and O-K edges (Egerton, 1996a).

Multiscattering effects due to the thickness of the specimen (100–150 nm) were observed on EELS spectra ($I_{plasmon}/I_{zero\text{-}loss}$ ratio = 0.5–0.6; ideally $I_{plasmon}/I_{zero\text{-}loss} < 0.1$). Nevertheless, no spectra deconvolution was systematically carried out. Because we determine relative proportions of elements, we chose to integrate all ionization edges with the same energy window Δ (with the exception of calcium, but it does not exceed 1% at. in the colloids). This method is recommended when ionization edges are of the same type (all K, or all L, or all M); then, multiscattering effects modify edge intensity in the same way (Egerton, 1996b) and concentrations can be obtained with a precision of ±1% (Leifer *et al.*, 2000). Nevertheless, this method can also be applied with success on K and L edges [Mavrocordatos & Perret, 1998 on a FeOOH system (Fe/O ratio), and Craven *et al.* (1997), on a TiN system (N/Ti ratio)], within 10–15% accuracy. Here, it was verified that good agreement was obtained between the ionization edges integration methods using the power-law model and using Fourier-ratio deconvolution. At 10 points along the profile, the edge intensities and resulting concentrations were evaluated using both methods; the results varied by less than 5%. The oxygen signal originating from the SiO supporting film was subtracted by collecting the signal of oxygen around the colloidal entities under identical conditions of analysis.

Results

Bulk chemical results

Our previous study (Mavrocordatos *et al.*, 2000) reports the physico-chemical changes between the peat pore water, the drain water and the river system. To summarize, in the peat, anoxic (< 1% O_2 saturation) and acidic (pH ≈ 4.5) conditions favour the stabilization of ferrous iron in solution ($[Fe^{2+}]_{peat} \approx 90\%$ of $[Fe_{tot}]$), whereas oxic (> 60% O_2 saturation) and neutral (pH ≈ 6.5) conditions, in the drain water, lead to a decrease of Fe^{2+} in the drain and in the river ($[Fe^{2+}]_{drain} \approx [Fe^{2+}]_{river} \approx 50$–$55\%$ of $[Fe^{2+}]_{tot}$). Oxidation of Fe(II) into Fe(III) lead to the formation of Fe(III) oxy(hydr)oxide colloids.

General microscopic survey using EDS

A first TEM-EDS approach allows us to distinguish clearly anoxic (peat) and oxic (drain) samples (Fig. 1). In the peat pore water, globular entities with a size range between 100 and 600 nm are observed. They exist as individual entities or agglomerated into assemblies (Fig. 1a,b) as revealed by two preparation methods; embedding in Nanoplast® resin under N_2(g) and direct ultracentrifugation on TEM grids. In drain samples, similar particles with a globular shape and a size ranging between 100 and 500 nm are detected (Fig. 1c). They are commonly observed as aggregates of three or four units.

Table 1. Relative proportions of elements obtained on globular entities in peat and drain specimens (the contribution of the sum of other trace elements, less than 1% at., is not reported here). EDS analyses were carried out on 40 colloids (< 500 nm) in each case. EELS line scan analyses were performed on two colloids (acquisition of ~250 spectra for each individual colloid). The mean and the standard deviation of these analyses are reported. For EELS analyses, the variability is related to the heterogeneity observed within each entity (Fig. 5), whereas for EDS analyses, the variation from one particle to another is taken as error bar.

Element proportion	C (% at.)	O (% at.)	Fe (% at.)	Ca (% at.)
Peat				
EDS	89 ± 4	10 ± 3	0.07 ± 0.03	1.1 ± 0.5
Drain				
EDS	60 ± 6	33 ± 4	5 ± 1	1.6 ± 0.2
EELS	64 ± 4	32 ± 3	3 ± 1	0.7 ± 0.4

The nature of the globular entities was first compared on the basis of their EDX spectra (Fig. 1(d)–(f)); whereas in the peat, globular colloids contain almost exclusively carbon, oxygen and calcium, in the drain, they also contain a large amount of iron. The morphological and analytical similarity of colloids in both peat specimens ensures that the ultracentrifugation procedure protects the sample from oxygenation and keeps colloids configuration. This is particularly important as this method is quantitative (i.e. colloids distribution on TEM grid is directly related to their concentration in solution) and induces less carbon background signal. To better understand the evolution of the globular colloids between peat and drain, the average element proportions on around 40 entities from each site were calculated (Table 1). The quantification confirms a net increase in iron content between peat and drain globules (from ~0.07–5% at.). Also, the results highlight the predominance of carbon and oxygen in the globular entities, even in the drain (C + O ~ 90% at.). As a result, iron and calcium are only minor elements, their contribution being less than 8% at. The sum of other trace elements (silicon, phosphorus, sulphur and aluminium) represents less than 0.5% at. in the peat globules and less than 1% at. in the drain globules. These observations suggest that globular organic-rich colloids, composed mainly of carbon and oxygen, are transported from the anoxic peat waters to the oxic drain waters, and act as condensation nuclei for the precipitation of amorphous iron oxy(hydr)oxides.

To assess the number proportion of Fe-rich colloids in the drain, we carried out a discrimination of particles by selecting

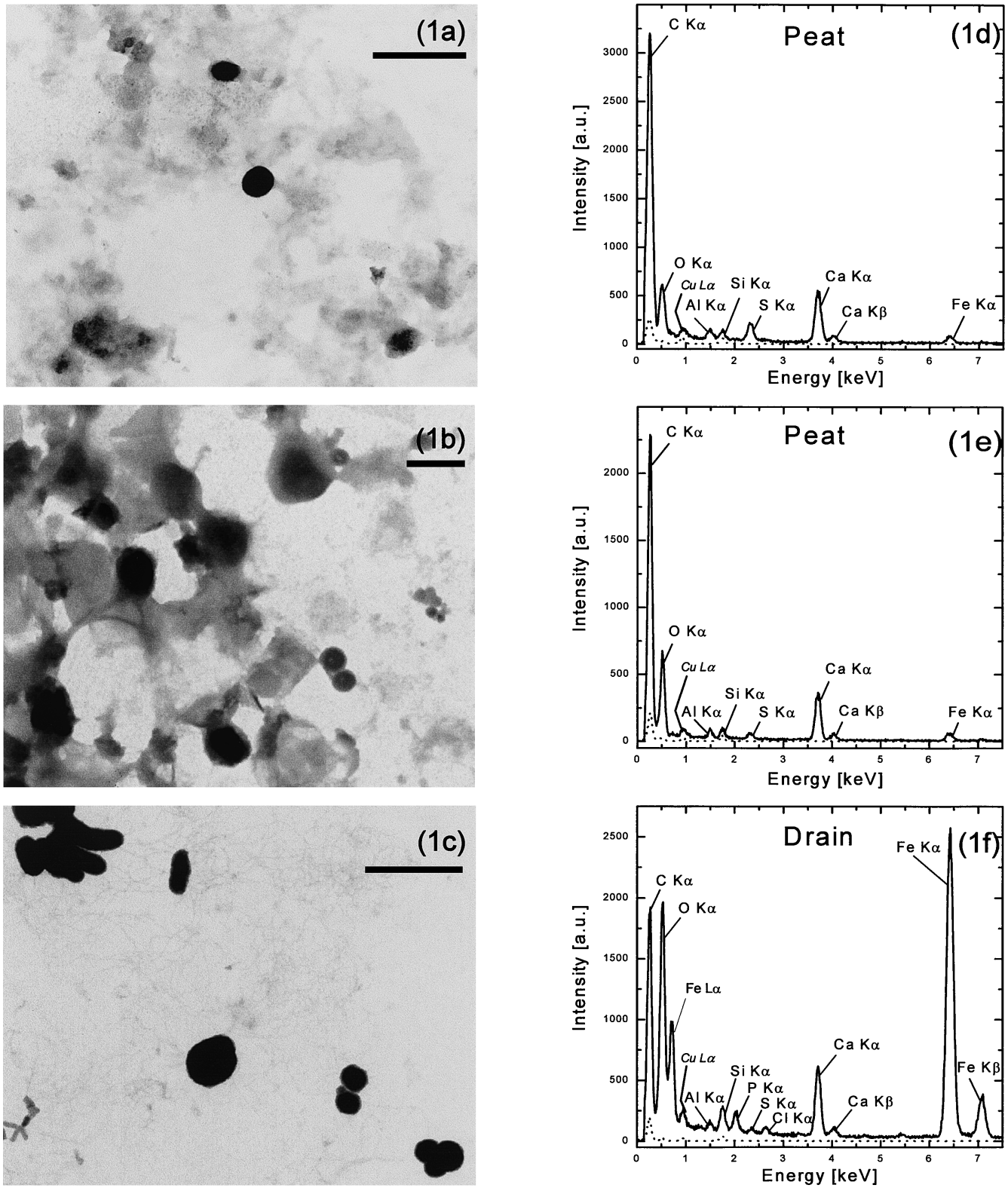

Fig. 1. Evolution of natural colloids between anoxic peat pore water and oxic drained water. TEM bright-field images and associated TEM-EDS spectra of (a, d) peat specimen prepared by embedding in Nanoplast® resin; (b, e) peat specimen and (c, f) drain specimen prepared by direct ultracentrifugation on TEM grids. Doted lines are TEM-EDS spectra collected under identical analytical conditions on colloid-free embedding medium and/or supporting film. The Cu peak originates from the TEM supporting grid. Scale bar = 500 nm.

Table 2. Classification of colloids in the drain specimens on the basis of their element composition determined by TEM-EDS and their size range (n = 79 entities analysed).

	Criterion	Average (% at.)	Number of analysed entities	Number proportion of entities in each size class [%]			
				< 0.5 μm	0.5–1 μm	> 1 μm	Σ =
OM			6	3.8	0	3.8	7.6
(C + O)	> 97% at.	98 ± 1					
C%		90 ± 3					
Fe%		0.4 ± 0.3					
OM-FeCa			64	50.6	15.2	15.2	81.0
(C + O + Fe + Ca)	> 97% at.	98.5 ± 0.2					
C + O		93 ± 1					
C%		67 ± 5					
Fe%		4 ± 1					
Clays			4	0	3.8	1.3	5.1
(Si + Al)	> 4% at.	11 ± 2					
(Si/Al)	< 3	2.2 ± 0.2					
(C + O)	< 90% at.	86 ± 2					
C%		56 ± 5					
Fe%		0.9 ± 0.1					
Clays-FeCa			4	1.3	1.3	2.5	5.1
(Si + Al)	> 4% at.	9 ± 4					
Si/Al	< 3	1.2 ± 0.4					
(Fe + Ca)	> 2% at.	3 ± 1					
(C + O)%		87 ± 4					
C%		57 ± 14					
Fe%		1.6 ± 0.8					
SiOx			1	0	0	1.3	1.3
Si	> 20% at.	21					
(C + O)%		77					
C%		29					
Fe%		0.9					
Σ =				55.7	20.3	24.1	100%

different classes of entities (79 entities analysed) with respect to their composition. The criteria chosen and the results obtained are reported in Table 2. Globular iron-containing colloids could be grouped in a homogeneous class, called OM-FeCa, for which C + O + Fe + Ca > 97% at. The group called OM (for organic matter) was identified by the high contributions of carbon and oxygen (C + O > 97% at.). In this class, contributions of other elements (silicon, iron, calcium and sulphur) are less than 1% at. each. Clay minerals have been identified by their content in silicon and aluminium and their Si/Al ratio. Their morphology (facetted borders) was also used as a selection criterion for this class. We also discriminated clays and aggregates formed by clays and OM-FeCa entities (Clays–FeCa). This association does not impair the morphology and the chemical composition of OM-FeCa colloids but it may drastically influence their transport behaviour in waters (Atteia *et al.*, 1998). Finally, entities are labelled SiO_x (for silicon oxide) when their silicon content is higher than 20% at. With this classification, it appears that the colloidal form of iron called OM-FeCa is predominant in the system, representing 81% of the analysed entities in the drain samples (86% when taking into account clays-FeCa colloids). This result emphasizes the systematic relation between iron and organic matter in the drain waters. In addition, the remarkable similarity in size and morphology of the globular OM and OM-FeCa entities found in the peat pore water (but still present in the drain; 7.6% of all entities) and those in the drain, strongly suggests that the latter are formed from the former.

Local analysis of individual colloids using electron energy-loss techniques

Further investigation was undertaken by electron energy-loss spectrometry in order to detail element distributions within

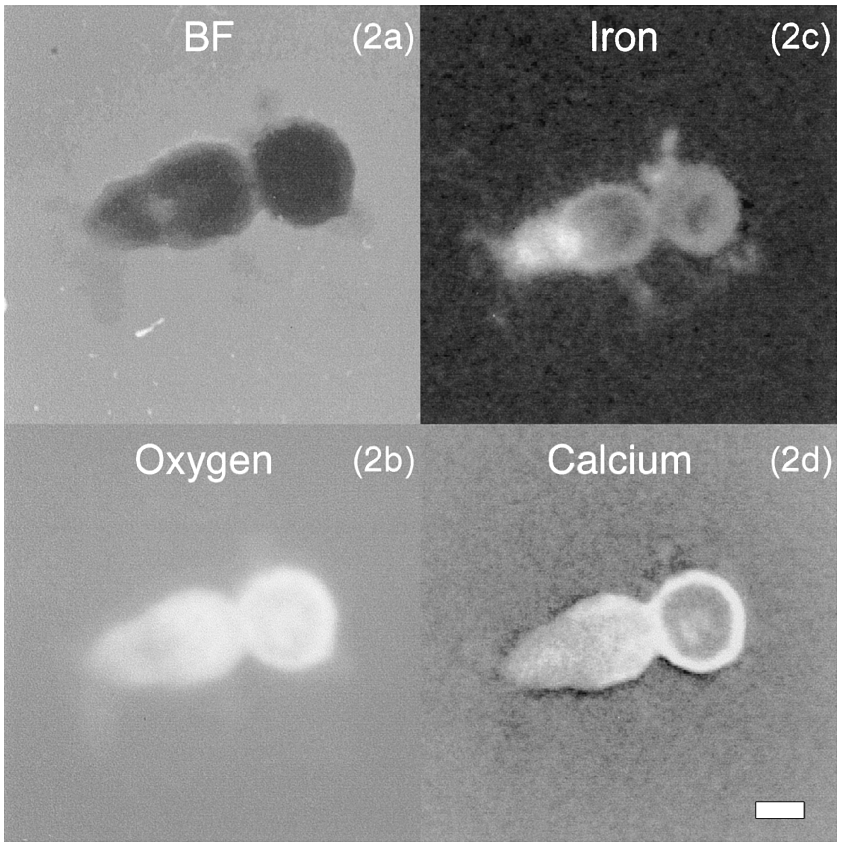

Fig. 2. (a) TEM bright-field image of an OM-FeCa colloid collected in the river water and (b, c, d) ESI images on O-K, Fe-$L_{2,3}$ and Ca-$L_{2,3}$ ionization edges, respectively. It was shown that drain and river colloids have a similar composition (Mondi, 1999). Scale bar = 100 nm.

OM-FeCa entities. Figure 2 shows the ESI images of iron, calcium and oxygen in an aggregate of two globules. In these chemical images, the presence of an element appears brightly. Heterogeneity in element distribution comes out: iron and calcium are preferentially localized on the border of the particles, whereas oxygen atoms are dispersed on the whole colloid. It follows that OM-FeCa colloids rise like an organic core surrounded by an iron and calcium rich shell. However, some precautions have to be taken for the interpretation of these results because of the specimen thickness and the thickness variation, which influence multiscattering effects and background parameters, respectively. Chemical images are thus taken only as an indication of element distribution on the whole OM-FeCa entities and will be strengthened by an EELS line-scans experiment. Acquiring EELS spectra on a specimen deposited on a carbon-free film first ensures the unequivocal presence of carbon in these globules. The use of a SiO supporting film requires special care as it was found to be unstable under the electron beam. Cooling the specimen not only limits radiation damage, but also protects the specimen from hydrocarbon contamination during microanalyses. A typical parallel-acquisition EELS spectrum (acquisition time ~ 1 s) represented on Fig. 3, shows distinctly the K ionization edges of carbon and oxygen and the $L_{2,3}$ ionization edges of iron and calcium, respectively.

The information obtained by TEM-EDS (Fig. 1), ESI (Fig. 2) and EELS (Fig. 3) strongly and correlatively suggest that the organic-rich globules found in the anoxic peat undergo chemical transformation when they are transported to the oxic drain, probably acting as condensation nuclei for the oxidation of Fe(II) followed by surface precipitation of Fe(III). To confirm this hypothesis, EELS line scans were recorded on two OM-FeCa globules extracted from the drain. As described above, spectra were recorded under non-disturbing conditions (short acquisition time; specimen cooling) every nanometre along the globules. It was then possible to extract element profiles (C, Ca, Fe, O) from EELS spectra along the globules. These profiles depend not only on the element distribution within the globules, but also on the thickness of the latter. A simple model was used to help interpret the variation of element proportions within the globules. Assuming homogeneously distributed elements in a spherical colloid, the number of atoms (or the corresponding signal intensity of the element) is weaker on the border of the particle, as represented on Fig. 4(a). By contrast, elements distributed homogeneously in a shell of constant thickness around an empty core yield a reduced signal in the centre of the colloid (Fig. 4b).

As represented on Fig. 5, for one of the drain globules analysed by line-scan EELS, we observe clear differences in element distributions. The distribution of carbon is in agreement with the 'solid sphere' model (Fig. 5a). In contrast, as previously suggested for the results obtained by ESI, iron and, to a lesser extent, calcium are preferentially localized at the outer

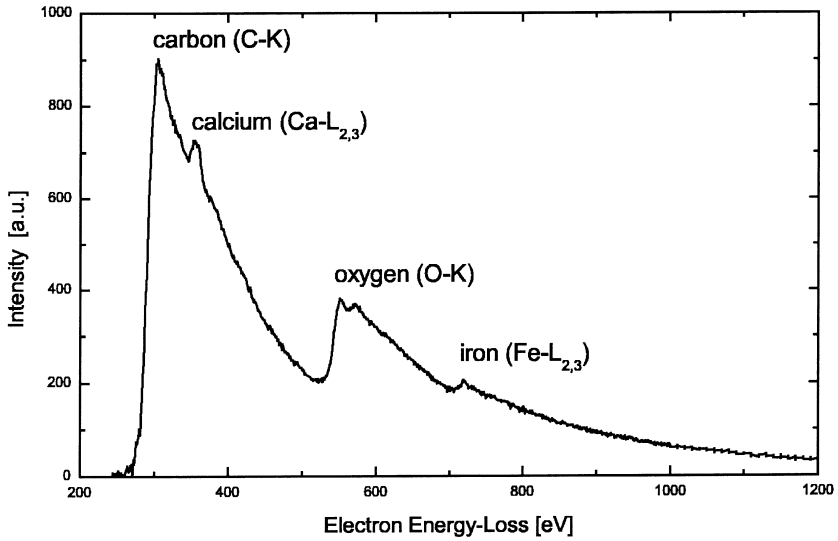

Fig. 3. A typical electron energy-loss spectrum, collected on a line across an OM-FeCa colloid, shows distinctly the K ionization edges of carbon and oxygen and the $L_{2,3}$ edges of iron and calcium. Background intensity was subtracted before carbon C-K ionization edge.

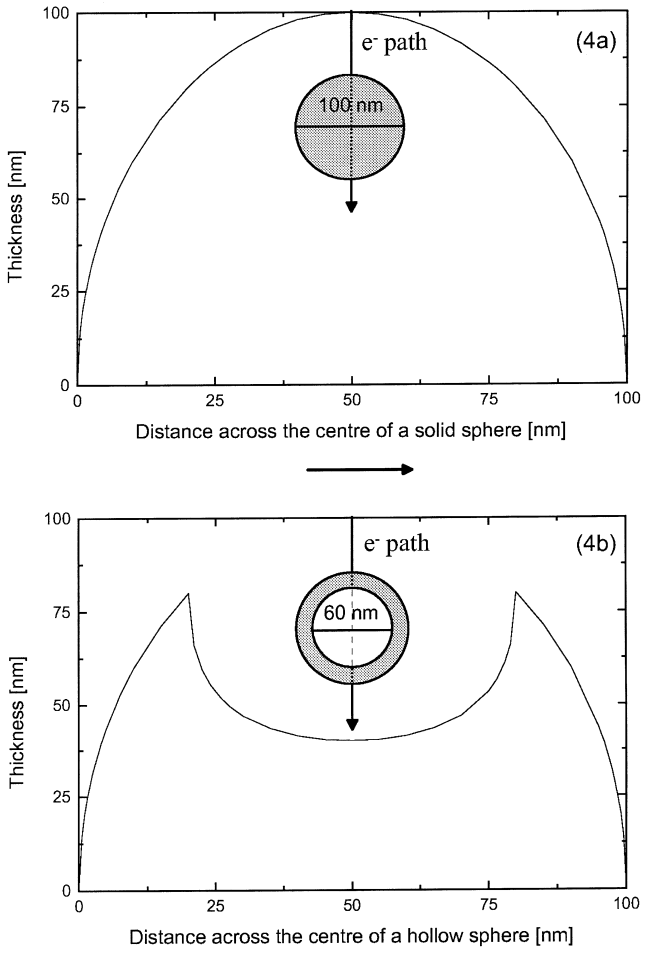

Fig. 4. Modelling of the thickness variation on a line passing through the centre of a sphere: (a) solid sphere with a 100 nm diameter). (b) sphere with an arbitrary empty core of 60 nm diameter.

sphere of the OM-FeCa colloid, in agreement with the 'hollow sphere' model (Fig. 5(b) and (d). The discrepancy between the left side (high iron and calcium signals) and the right side (weaker iron and calcium signals) of the line scan shows that their atomic distribution is not symmetric and homogeneous within the globule. These differences were not detected on ESI images, which do not attain such a high spatial resolution in our experiment. Finally, the signal of oxygen is more difficult to interpret, as this element is present both in the supporting film (SiO), in the organic rich core ($C_xH_yO_z$), and in the Fe-rich ($Fe_xO_y(OH)_z$) outer crust (Fig. 5c). These results are in full agreement with the hypothetical model of an organic core surrounded by iron precipitates. Carbon and oxygen, the major components of organic matter, form the core of the OM-FeCa colloids. The preferential occurrence of iron and calcium at the outer sphere is discussed later.

A detailed investigation of EELS line scans at the nanometre scale brings supplementary information on the repartition of atoms within the globules. Carbon, iron and calcium present strong intensity variations along the profile (Fig. 5(a), (b) and (d)). These intensity variations correspond to variations in the number of atoms from one position to another ($\Delta x = 1$ nm), because they are clearly larger than the statistical fluctuations in the first 20 nm of the profile (i.e. in the vicinity of the particle; not shown). Spectacularly, we observe a systematic anti-correlation between iron and carbon; each iron peak (width between 7 and 23 nm) corresponds to a reduction of the carbon intensity. This observation is of the utmost importance as it highlights the presence of iron-rich nano-areas that exclude carbon. As mentioned above, the overlap between the Ca-$L_{2,3}$ edge and C-K post-edge background leads to a systematic error in the calculation of calcium concentration. Nevertheless, Fig. 5 shows that calcium follows the general trend of iron, even if calcium is only semi-quantitative. In other words, lower local concentrations of carbon are correlated to higher local concentrations of iron and calcium, respectively.

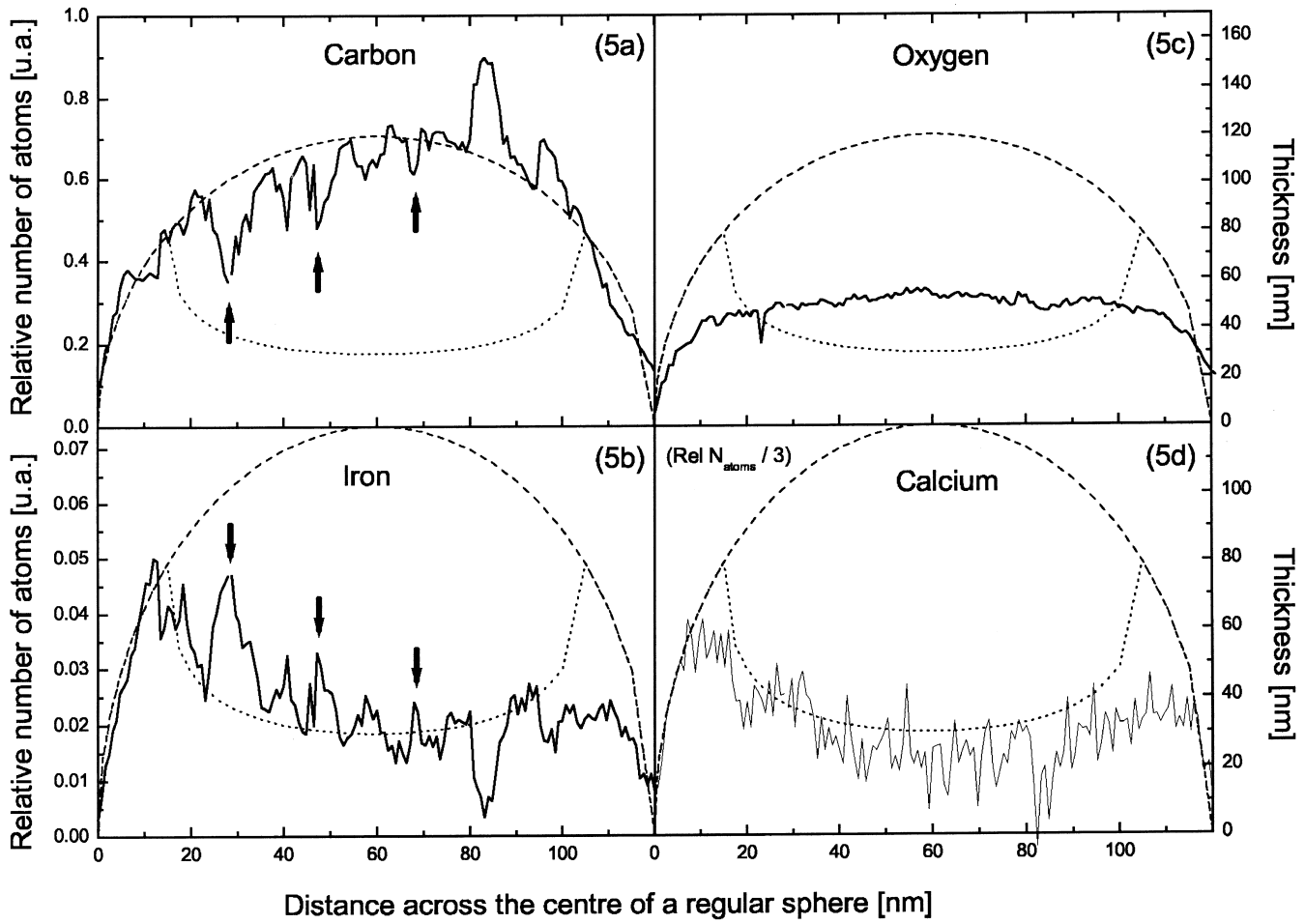

Fig. 5. EELS line scan signal intensity evolution across a small OM-FeCa colloid (~120 nm; spectra were recorded each nanometre). The dashed and the dotted lines, as guides for the eyes, correspond to the thickness evolution of a plain, respectively, a hollow sphere surrounded by a crust of constant thickness (see Fig. 4). The arrows emphasize local iron enrichments (between 7 and 23 nm). Signal contribution coming from the SiO TEM grid supporting film was subtracted.

The average composition of the two colloids analysed by line-scan EELS was calculated by integrating the signal over the entire globules. The results, given in Table 1, compare well with the EDS results obtained on 40 globules. In both cases, carbon and oxygen predominate (C + O ~ 93% at. by EDS; 96% at. by EELS), whereas iron and calcium represent minor elements (Fe + Ca ~ 6.6% at. by EDS; 3.7% at. by EELS).

Discussion

The precipitation of iron in natural waters usually leads to mixtures containing other elements (Cornell & Schwertmann, 1996; Rose *et al.*, 1996; Lienemann *et al.*, 1999). For several years, the thorough use of analytical electron microscopy for the characterization of natural colloids has dramatically broadened our knowledge on their formation pathways, characteristics and behaviour. For instance, the work of Perret *et al.* (2000) illustrates the role of organic matter on the morphotypes of natural hydrous iron oxides in different aquatic systems: apparently, the nature of the organic matter, as well as its concentration and the bulk physico-chemical conditions of the milieu, are the main influential parameters.

Our study fits within this frame. We focused our interest on a complex redox transition interface (peat-drain), where iron precipitation is favoured by the oxygenation of the peat pore water and the rapid pH increase in the presence of high concentration of humic substances coming from the peat soils (Gobat *et al.*, 1998). Humic substances (humic acids, HA) are high molecular weight organic macromolecules formed from the biochemical degradation of plant and animal remains. Although they present a high heterogeneity, they have properties in common: their propensity to aggregate (Ghosh & Schnitzer, 1980; Leppard *et al.*, 1986); and their complexation properties towards cations (Stumm & Morgan, 1996). Amongst others, they are known to stabilize iron cations (HA-Fe^{2+}, HA-Fe^{3+}) in solution (Luther *et al.*, 1992; Shaw, 1994).

In our study, analytical electron microscopy shows that humic substances also act as nucleation sites for the formation of iron oxy(hydr)oxide.

Humic substances exhibit a broad variety of macromolecular structures and compositional differences in aqueous solution, depending on the bulk physico-chemical conditions. A globular configuration, described in different natural and laboratory systems (Myneni *et al.*, 1999), is related to aggregation processes. The formation of such dense aggregates implies a neutralization of the charges in the inner organic sphere, with a resultant inhibition of repulsive interactions. At the opposite, negatively charged hydrophilic groups are preferentially situated at the outer sphere, and contribute to the stabilization of the aggregates in water. As a consequence, the surface area of globular humics is highly reactive with respect to cation complexation processes.

In the peat pore water of the Vallée-des-Ponts, acidic conditions (pH ≈ 4.5) and a high concentration of organic matter ([OM] ≈ 50 mg C/L) favour the aggregation of humic substances. AEM highlights the presence of very dense organic colloids ranging in size between 100 and 600 nm. Chemical speciation calculations (not shown, ECOSAT; Keizer & van Riemsdijk, 1998) indicate that ferrous iron, as well as calcium, can be found either as free ions or complexed to organic matter in solution. AEM confirmed this assumption by detecting only minor or trace proportions of both elements in the organic colloids (< 1 at%; Table 1). After oxidation of the peat pore water transported to the drain, an immediate solution supersaturation theoretically occurs with respect to ferrihydrite (an amorphous iron hydroxide, generally occurring as primary phase), whereas the chemistry of calcium remains unchanged. In our drain samples, we distinguished only one type of iron-rich precipitate in the form of globular entities, called OM-FeCa. Surprisingly, these globules bear a strong similitude (size, morphology and composition) with the globular organic colloids found in the peat. The occurrence of iron precipitation in the drain is shown by the net increase in iron within the globules (Fe/C atomic ratio increases by approximately 100× between peat and drain globules), whereas calcium remains stable. Line scan PEELS data of drain globules yield a similar distribution of iron and calcium at the nanometre-scale, suggesting that adsorption sites on the globules originating from the peat are involved in the nucleation and precipitation of iron in the drain.

The presence of iron oxy(hydr)oxide nanoparticles (2–3 nm) on organic surfaces (i.e. thin stalk-like and sheath-like bacteria) was described recently by Banfield *et al.* (2000). They suggest an additional self-assembly based coarsening mechanisms, i.e. iron nanoparticles would form in solution and either flocculate to form larger aggregates or attach to surfaces of bacteria (carrying negatively charged exopolymers). Likewise in our samples, line scan PEELS data highlight the presence of iron aggregates of nanometric size range on an organic core. Such results are particularly relevant for the understanding of colloids reactivity. Surfaces of iron oxy(hydr)oxides in the environment are active adsorption sites (e.g. for arsenate or phosphate in acidic solutions and metals in alkaline solutions). When they occur as nano-aggregates, their area per given volume ratio increases significantly, as well as their adsorption site number.

Conclusions

The understanding of the formation pathway of iron oxy(hydr)oxide colloids, at the interface between the anoxic peat pore water and the oxygenated drain water in the Vallée-des-Ponts, had to overcome several difficulties with respect to the origin of our natural samples: qualitative and quantitative representativity of the observed Fe-rich particles and identification of organo-mineral mixed phases. The combination of both micrometre- and nanometre-scale EDS and EELS analyses helped us to overcome these difficulties. First, a global approach was performed by means of TEM-EDS analyses. It was established that a unique form of globular iron precipitate is present in the oxygenated waters. In addition, the unexpectedly high proportion of organic matter in these iron colloids, as well as their morphology and size range, allowed us to correlate them with the purely organic globules identified in the peat. This global approach proved to be very efficient to reveal the complex formation pathway of OM-FeCa colloids.

In addition, EELS analyses and ESI images were used to detect local changes within globules at the nanometre-scale. Irregularities in the element distributions were hightlighted with a spatial resolution of around 1 nm (EELS line scans). Our most important contribution is the identification of nanometre-sized iron enrichments preferentially localized at the outer sphere of the organic entities. EELS in line scan mode was particularly well suited for this identification: compared to EDS, its higher detection efficiency for light elements allowed unequivocal quantification of carbon in the globules, under non-disturbing conditions (short acquisition time; specimen cooling). Our data strongly support the role of the peat organic globules for iron precipitation. To our knowledge, such observations had not been made before in soil solution, they represent a crucial breakthrough for the understanding of the formation processes of complex particles. The nature of the organic matter involved in the process must certainly be ascertained, although humic substances are the most probable candidates.

Acknowledgements

This study was carried out with the financial support of the Swiss National Science Foundation (#20-42250.94; #21-43438.95). We wish to thank P. Stadelmann (Swiss Federal Institute of Technology, Lausanne, Switzerland) and S. Fakan (University of Lausanne, Switzerland) for access and support on AEM, and M. F. Benedetti (UMR CNRS 7047) for chemical speciation calculations.

References

Atteia, O., Couture, C. & Perret, D. (1998) Factors controlling colloidal transport in a karst aquifer. *Phys. Chem. Earth*, **23**, 163–169.

Atteia, O. & Kozel, R. (1997) Particle size distributions in waters from a karstic aquifer: from particles to colloids. *J. Hydrol.* **201**, 102–119.

Bachhuber, K. & Frösch, D. (1983) Melamine resins, a new class of water-soluble embedding media for electron microscopy. *J. Microsc.* **130**, 1–9.

Banfield, J.F., Welch, S.A., Zhang, H., Ebert, T.T. & Penn, R.L. (2000) Aggregation-based crystal growth and microstructure development in natural iron oxy(hydr)oxide biomineralization products. *Science*, **289**, 751–754.

Cornell, R.M. & Schwertmann, U. (1996) *The Iron Oxides: Structure, Properties, Reactions, Occurrence and Uses*. VCH, Weinheim.

Craven, A.J., Kejian, H. & Baker, T.N. (1997) The use of PEELS for the study of precipitate complexes in HSLA steels. *Institute Phys. Conference Ser. Electron Microscopy and Analysis Group Conference EMAG97, Cambridge*, pp. 605–608.

Egerton, R.F. (1996a) Quantitative analysis of the energy-loss spectrum. *Electron Energy-Loss Spectroscopy in the Electron Microscope*, 2nd edn. Plenum Press, New York.

Egerton, R.F. (1996b) Quantitative analysis of the energy-loss spectrum. *Electron Energy-Loss Spectroscopy in the Electron Microscope*, 2nd edn. Plenum Press, New York.

Ghosh, K. & Schnitzer, M. (1980) Macromolecular structures of humic substances. *Soil Sci.* **129**, 266–276.

Gobat, J.-M., Aragno, M. & Matthey, W. (1998) *Le Sol Vivant*. Presses Polytechniques et Universitaires Romandes, Lausanne.

Keizer, M.G. & van Riemsdijk, W.H. (1998) *ECOSAT: Equilibrium Calculation of Speciation and Transport. User Manual, Version 4.* Wageningen Agricultural University, Wageningen.

Leifer, K., Buffat, P.A., Stadelmann, P.A. & Kapon, E. (2000) Theoretical and experimental limits of the analysis of III/V semiconductors using EELS. *Micron*, **31**, 411–427.

Leppard, G.G., Buffle, J. & Baudat, R. (1986) A description of the aggregation properties of aquatic pedogenic fulvics acids. *Wat. Res.* **20**, 185–196.

Lienemann, C.-P., Heissenberger, A., Leppard, G.G. & Perret, D. (1998) Optimal preparation of water samples for the examination of colloidal material by transmission electron microscopy. *Aquat. Microb. Ecol.* **14**, 205–213.

Lienemann, C.-P., Monnerat, M., Dominik, J. & Perret, D. (1999) Identification of stoichiometric iron-phosphorus colloids produced in a eutrophic lake. *Aquat. Sci.* **61**, 133–149.

Luther, G.W., Kostka, J.E., Church, T.M., Sulzberger, B. & Stumm, W. (1992) Seasonal iron cycling in the salt-marsh sedimentary environment: the importance of ligand complexes with Fe (II) and Fe (III) in the dissolution of Fe (III) mineral and pyrite, respectively. *Mar. Chem.* **40**, 81–103.

Mavrocordatos, D., Mondi-Couture, C., Atteia, O., Leppard, G.G. & Perret, D. (2000) Formation of a distinct class of Fe-Ca (-C_{org})-rich particles in a complex peat-karst system. *J. Hydrol.* **237**, 234–247.

Mavrocordatos, D. & Perret, D. (1998) Quantitative and qualitative characterization of aquatic iron oxyhydroxide particles by EF-TEM. *J. Microsc.* **191**, 83–90.

McCarthy, J.F. & Degueldre, C. (1993) Sampling and characterization of colloids and particles in groundwater for studying their role in contaminant transport. *Environmental Particles* (ed. By J. Buffle and H. P. van Leeuwen), Vol. 2, pp. 247–315. Lewis Publishers, Boca Raton, FL.

Mondi, C. (1999) Formation et devenir de colloïdes associant matière organique et fer dans les eaux drainant les tourbières d'un bassin karstique: étude physico-chimique et microscopique. PhD Dissertation, University of Lausanne, Lausanne.

Myneni, S.C.B., Brown, J.T., Martinez, G.A. & Meyer-Ilse, W. (1999) Imaging of humic substance macromolecular structures in water and soils. *Science*, **286**, 1335–1337.

Perret, D., Gaillard, J.-F., Dominik, J. & Atteia, O. (2000) The diversity of natural hydrous iron oxides. *Environ. Sci. Technol.* **34**, 3540–3546.

Perret, D., Leppard, G.G., Müller, M., Belzile, N., De Vitre, R. & Buffle, J. (1991) Electron microscopy of aquatic colloids: non-perturbing preparation of specimens in the field. *Water. Res.* **25**, 1333–1343.

Reimer, L. (1995) Electron Spectroscopic Imaging. *Energy-Filtering Transmission Electron Microscopy* (ed. By L. Reimer), pp. 357–400. Springer, Berlin.

Rose, J., Manceau, A., Bottero, J.-Y., Masion, A. & Garcia, F. (1996) Nucleation growth mechanisms of Fe oxyhydroxide in the presence of PO_4 ions. 1. Fe K-edge EXAFS study. *Langmuir*, **12**, 6701–6707.

Shaw, P.J. (1994) The effect of pH, dissolved humic substances, and ionic composition on the transfer of iron and phosphate to particulate size fractions in epilimnetic lake water. *Limnol. Oceanogr.* **39**, 1734–1743.

Stumm, W. (1993) Aquatic colloids are chemical reactants: surface structure and reactivity. *Colloid Surf. A*, **73**, 1–18.

Stumm, W. & Morgan, J.J. (1996) *Aquatic Chemistry*, 3rd edn. Environmental Science and Technology Series. Wiley-Interscience, New York.

Tessier, A. (1992) Sorption of trace elements on natural particles in oxic environments. *Environmental Particles* (ed. By J. Buffle and H. P. van Leeuwen), Vol. 1, pp. 425–453. Lewis Publishers, Boca Raton, FL.

Williams, D.B. & Carter, C.B. (1996) Quantitative X-ray microanalysis. *Transmission Electron Microscopy. A Text Book for Materials Sciences*. Plenum Press, New York.